Journal of Vacuum Science and Technology B

RESEARCH ARTICLE | OCTOBER 12 2023

In situ metrology of direct-write laser ablation using optical emission spectroscopy

Briana Cuero ; Kun-Chieh Chien ; Chih-Hao Chang

J. Vac. Sci. Technol. B 41, 062603 (2023)
https://doi.org/10.1116/6.0003031

JVST B
Journal of Vacuum Science & Technology B

ARTICLE

pubs.aip.org/avs/jvb

In situ metrology of direct-write laser ablation using optical emission spectroscopy

Cite as: J. Vac. Sci. Technol. B **41**, 062603 (2023); doi: 10.1116/6.0003031
Submitted: 1 August 2023 · Accepted: 21 September 2023 ·
Published Online: 12 October 2023

Briana Cuero, Kun-Chieh Chien, and Chih-Hao Chang[a)]

AFFILIATIONS

Walker Department of Mechanical Engineering, The University of Texas at Austin, Austin, Texas 78712

Note: This paper is part of the Special Topic Collection: Papers from the 66th International Conference on Electron, Ion and Photon Beam Technology and Nanofabrication (EIPBN 2023).

[a)]**Author to whom correspondence should be addressed:** chichang@utexas.edu

ABSTRACT

Direct-write laser ablation is an effective manufacturing method for etching complex microscale patterns, especially on hard ceramics such as sapphire that are difficult to machine using traditional mechanical or micromachining methods. However, the variability of the laser–matter interaction causes inconsistencies that prevent this process from moving beyond the research realm. This work presents the real-time monitoring of the ablation process in sapphire using optical emission spectroscopy to assess the key wavelengths that exhibit strong correlations to the fabricated features. In this process, a focused ultrafast laser is used to create microscale features and morphological changes in sapphire substrates, which are studied by a subsequent wet etching in a hydrogen fluoride solution. The etched sapphire samples are observed to have amorphous sapphire removed, resulting in microstructures with higher profile fidelity. Furthermore, principal component analysis of the measured spectral obtained during the etch process indicates that the emission from a few key wavelengths exhibits strong correlations to the etched sapphire patterns. This result indicates that the use of data-driven techniques to assess the spectral emissions of direct-write laser ablation can be a useful tool in developing *in situ* metrology methods for laser-matter interactions.

I. INTRODUCTION

Direct-write laser ablation is a powerful tool for microscale rapid prototyping and can create intricate designs in inorganic materials such as metals,[1] glass,[2] and sapphire.[3] These designs can have more complex features that are challenging or impractical to be obtained by traditional microscale patterning and can reduce energy and material waste during the manufacturing process. Although current processes have demonstrated effective patterning, there lies an issue in how the process parameters can be better controlled in real time to obtain higher pattern repeatability. In previous studies, process data such as high-speed imaging[4] and temperature[5] are collected for process control and quality monitoring. Among these techniques, optical emission spectroscopy (OES), which analyzes the light emitted during laser ablation, provides a valuable solution for process control and monitoring due to its noncontact measurement, real-time implementation, and robustness to environmental noises. In these techniques, optical emission is induced by element-specific light moving from higher to lower electron energy levels and can provide useful information about the elemental composition of ablated materials.

Previous work involved in the metrology of direct-write laser ablation has attempted to integrate optical instruments in the system to monitor the emitted light that emits when the laser interacts with the material. This has been achieved through *in situ* optical emission spectroscopy[6,7] or pyrometry.[8] However, while the data from these methods are useful, the metrology of direct-write laser ablation currently lacks a discussion for selecting key emission wavelengths, which is typically based on elemental maps, physical models, and user experience. The goal is to select wavelengths that have critical process information for direct-write laser ablation, which is generally not trivial since the light-matter interactions are complex and difficult to model. Key wavelength selection is essential in *in situ* process monitoring because it is impractical to consider all wavelengths in the measured OES spectra for this purpose.

Direct-write laser ablation provides the opportunity to develop patterns in a myriad of materials and environmental conditions. Laser ablation is especially useful for the patterning of hard

ceramics such as sapphire,[9–12] which is difficult to micromachine using traditional mechanical or etching processes due to its high chemical stability and mechanical hardness. Sapphire has many applications such as photonics and optoelectronics because of its attractive mechanical, optical, and thermal properties. At the microscale, producing precise structures for applications such as biomimicry, micro-lenses, etc., in hard crystalline materials like sapphire generally requires the lithography process to generate desired patterns precisely on the sapphire surface. Subsequently, the pattern is transferred into the sapphire substrate using the etching process.[12] However, since sapphire is a chemically stable material with a low etch selectivity, these approaches are either relatively complicated[13–15] or results in simple patterns with a low aspect ratio.[16,17] On the other hand, studies demonstrate that high aspect ratio sapphire microstructures can be fabricated by direct-write laser ablations.[18] Moreover, combining direct-write laser ablation with wet etching processes can improve the fabrication efficiency by removing the amorphous region caused by the laser ablation. A recent study demonstrated that by using direct-write laser irradiation followed by a Cl_2/BCl_3 plasma etching to engrave compound eyes structures on the curved sapphire substrate, process efficiency can be enhanced by over two orders of magnitude.[14] However, the relationship between the parameters of the laser ablation system and the resultant morphology and pattern of the substrate is not well understood, presenting a challenge for process control.

This work presents the study of the emitted spectral information during direct-write laser ablation and the use of data-driven approaches to identify the key wavelength. The goal of this work is to demonstrate that OES signals can be monitored in real time to improve patterning accuracy and precision. The sapphire nanostructures studied in this work are patterned using ultrafast laser to induce ablation or morphological changes, the latter of which can be removed using a subsequent hydrogen fluoride (HF) etching. The samples are then analyzed before and after the HF etching using scanning electron microscopy (SEM) to examine the effects of the laser power on the sapphire ablation process. The measured dimensional data are compared with the OES data with principal component analysis (PCA) to identify key wavelength that exhibits strong correlation to the patterned sample features. This data-driven wavelength identification process does not rely on any user inputs and instead focuses on identifying data trends that exhibit strong correlations. The results indicate that the emission from a few key wavelengths can offer a strong prediction of fabricated feature width and depth with R^2 of 73% to 95%, respectively. This work demonstrates that the OES signal can be analyzed using data-drive methods to provide important laser ablation data in real time, which can lead to real-time metrology and process control of direct-write laser processes. This research can lead to precisely patterned sapphire nanostructures and find applications in nanophotonics,[19] functional sapphire windows,[20] and micromachining on flexible substrates.[21]

II. EXPERIMENT

A. Laser and metrology system setup

The laser ablation system used in this study is shown in Fig. 1, where the write process is monitored using OES. The laser used is

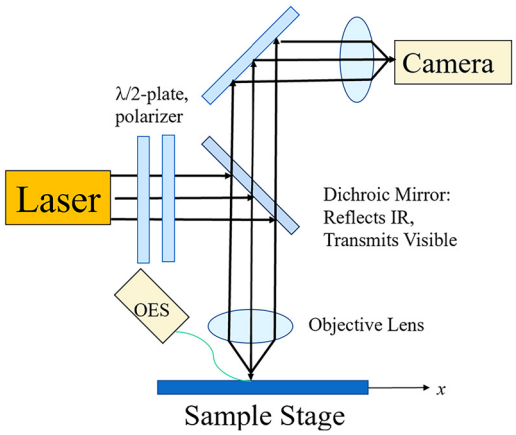

FIG. 1. Schematic of the laser ablation system with an ultrafast Ti: sapphire laser with an optical fiber to collect the emitted light for OES.

an ultrafast laser (Spectra-Physics Solstice Ace) with 40 fs pulses at 790 nm, and ablation experiments were performed at nominal power between 6 and 8 mW, at a repetition rate of 1 kHz, and a write speed of 200 μm/s. To determine the best position to capture the emission signal, an optical fiber is carefully positioned to ensure that the fiber is in the beam path of the emitted light and collects a sufficient amount of signal in the UV to visible range between 200 and 650 nm. A short wavelength filter is used to filter out the light around the laser line at 790 nm, which results in strong scattering from the sample and can saturate the spectrometer. The OES signal was collected by using an optical fiber with a collimating lens and a spectrometer (Ocean Insight HR4Pro) with wavelength ranging from 200 to 800 nm. The laser is focused by an objective lens to create a 6 μm spot at the substrate plane, which is mounted on a translational *x*-*y* stage for direct-write patterning. Direct measurement of the laser emission at the ablation spot is more accurate than monitoring the laser power at the source since optical losses can occur in the optical system.

The substrates for this experiment are double-side polished crystalline C-plane sapphire. The write pattern consists of a set of lines that with a length of 5 mm and spaced apart by 700 μm to ensure that the neighboring ablation lines do not overlap with one another. The ablation process can pattern more complex patterns by scanning the x-y stage. Therefore, the process is quite versatile and can pattern arbitrary 2D patterns. Furthermore, it is expected that multiple scans at a single point will have more material removed and the profile to deepen if the depth is within the depth of focus for the microscope objective. The laser power used is approximately 7.9 mW and is reduced for each line to examine the effect of the ablation power. The sapphire samples are ablated with 5–100% of the nominal power with 5% power increments, controlled using a rotating half-wave plate and a linear polarizer. Depending on the power and write speed, the sapphire surface can be ablated to create surface microstructures. For regions below the ablation power threshold, the material morphology can be changed to amorphous due to electronic excitation.[13] The amorphous phase

can be removed using wet etching, allowing features with finer fidelity to be patterned at below the ablation threshold.

After the substrate is patterned using the direct-write laser setup, the sample is cleaved to keep one half separate from the chemical etchant to establish the initial state of the substrate prior to postprocessing. The etched half of sapphire was etched in 49% HF solution for 10 to 20 min and rinsed in deionized water to etch away amorphous alumina and remove any free-floating particles. The samples before and after the HF etch are examined with SEM, where the width, depth, and the amorphous area are measured using ImageJ. The depth of the sample is measured from the edge of the sample to the edge of the shallowest parabolic depth. Once all physical measurements have been performed, the measurement data and the OES data are compared to determine a correlation between the morphology of the substrate before and after HF etching, as described further in Secs. II B–IV.

B. Principal component analysis

The correlation of the measured OES spectra and the fabricated pattern geometry is examined using principal component analysis (PCA),[22,23] which is a frequently employed technique in multivariate analysis for reducing dimensionality. It involves projecting correlated data onto a smaller set of uncorrelated data, thereby reducing data size. Simultaneously, PCA aims to retain the maximum amount of variation present in the dataset. Given an OES dataset X, which is a $m \times n$ matrix of m timestamps and n wavelengths, via PCA, X can be composed of the product of the score matrix T and the loading matrix W with an unmodeled residual matrix E:

$$X = TW^T + E, \tag{1}$$

where

$$T = [t_1, t_2, \ldots, t_l], \tag{2}$$

$$W = [w_1, w_2, \ldots, w_l]. \tag{3}$$

Here, ls the number of principal components, which is normally much less than n. TW^T represents the PCA-modeled component. The loading matrix W consists of eigenvectors acquired through the eigendecomposition of the covariance matrix of the OES data X. Because both the score matrix T and the loading matrix W are orthogonal, Eq. (2) can be reformulated as

$$t_k = X \cdot w_k, \quad \text{where } k \leq l. \tag{4}$$

In Eq. (4), the score vector t_k represents the projection of the original OES data X onto the k^{th} principal component. Consequently, the loading vector w_k indicates the contribution of each wavelength in forming the score vector t_k. As loadings can have positive or negative values, squared loadings are utilized to identify significant emission wavelengths in the OES data. Higher squared loadings correspond to greater importance for the corresponding wavelength. Previous studies[24,25] demonstrated that, via PCA, key emission wavelengths of the OES data in the plasma etching process can be identified.

Therefore, instead of picking the strongest emission in the raw OES data, using PCA helps to identify which wavelengths contribute more to the variance of the OES data caused by different doses. In this work, the wavelength that exhibits the strongest emission and the key wavelengths selected based on squared loadings obtained from PCA versus different doses will be discussed. Furthermore, the relationship between the emission intensity versus line width and depth before and after the HF etching will be investigated.

III. RESULTS AND DISCUSSION

A. Sapphire ablation and etching

The results of the sapphire patterning process using the ultrafast laser are shown in the cross-sectional scanning electron microscope (SEM) images in Fig. 2. The sample ablated at a dose of 37.6 J/cm^2 is shown in Fig. 2(a), and the depth, width, and amorphous area of the patterned feature are clearly defined. The morphology of the sample after laser ablation is occluded by a

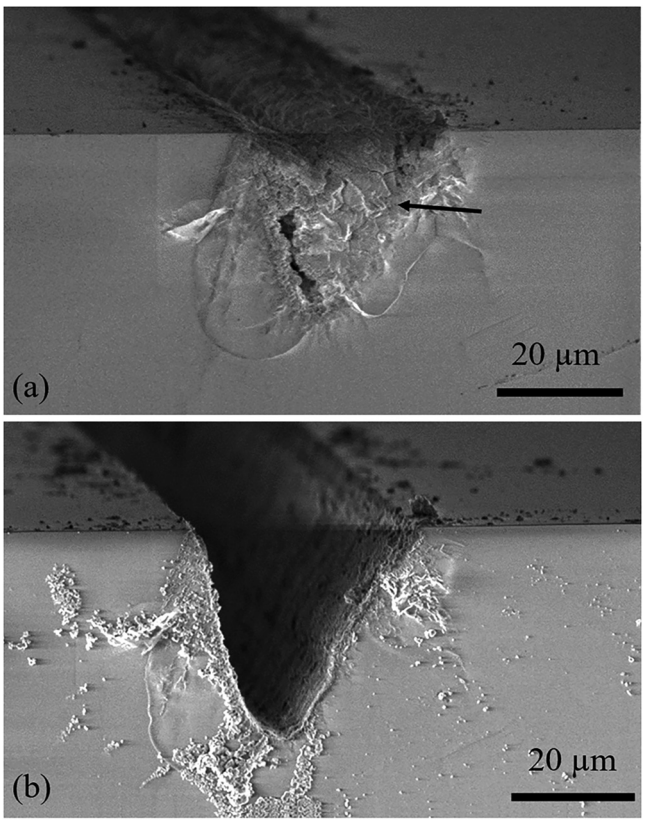

FIG. 2. Cross-section SEM images of sapphire samples ablated a dose of 37.58 J/cm^2 (a) before and (b) after 10 min in HF solution. The arrow indicates the remaining amorphous alumina region.

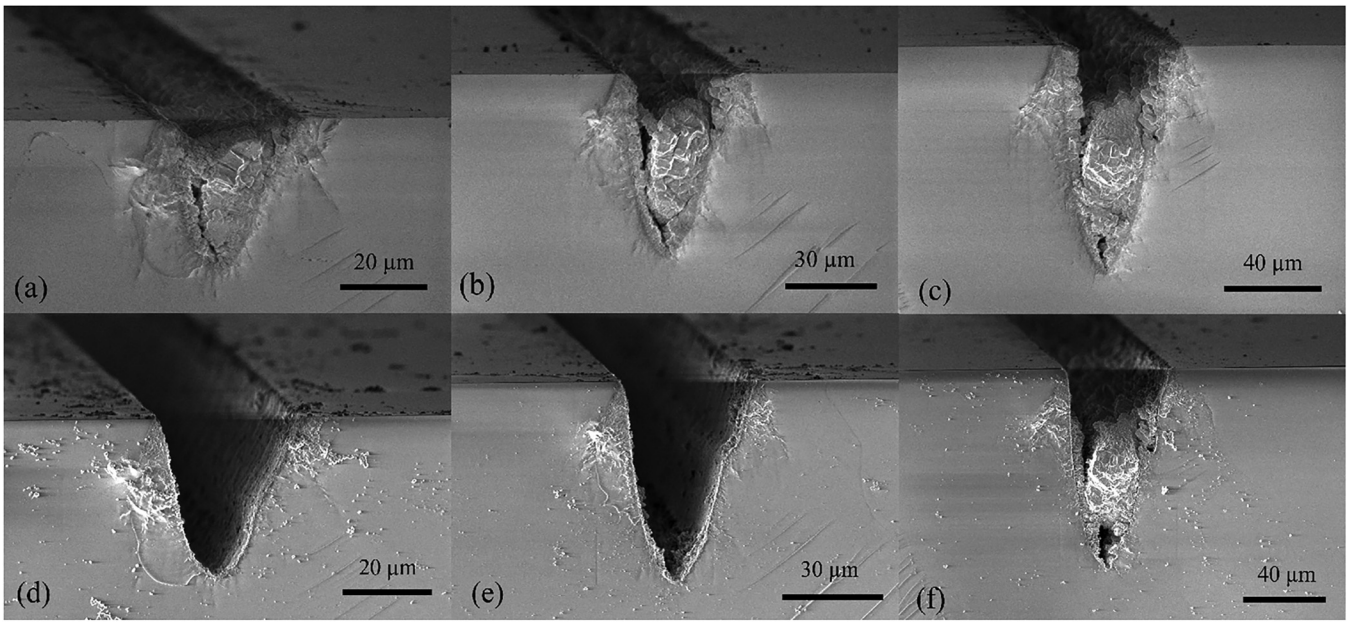

FIG. 3. Cross-section SEM images of sapphire samples ablated as doses of (a) 43.0 J/cm^2 (b) 85.9 J/cm^2, (c) 172 J/cm^2 before HF etching. The corresponding cross-section SEM images of the samples after 10 min of HF etching are shown in (d)–(f), respectively.

substantial amorphous area, as denoted in the figure. It can be observed that the feature depth immediately after patterning is quite shallow, since the ablation threshold has not been reached across the whole region due to the relatively low dose. After the etching in HF solution for 10 min, the amorphous alumina region has been completely removed, as shown in Fig. 2(b). Here, it can be observed that the feature forms a well-defined parabolic trough. It is also interesting to note that while the profile fidelity has improved, there is residual debris on the surface that remains on the surface. This can be attributed to the crystalline morphology of the particles, which etches slower than amorphous alumina. The debris can possibly be removed using ultrasonic agitation or HF etch at elevated temperature.

Additional samples have been fabricated using a wide power range, and the fabricated structures for 43.0, 85.9, and 172 J/cm^2 are shown in Fig. 3. It can be observed that all the samples before and after etching have similar key features. A notable feature is the depth and profile of the pattern line, which has a parabolic shape that emulates that of the focal point of the laser. The focus of the laser system in this experiment is performed manually, which introduces the potential for the parabolic shape to shift in the depth direction depending on minute changes to the focus. The sapphire substrate used can also have substrate warpage on the order of a few micrometers, which can further contribute to defocusing. It can be estimated that the focal plane is between 8 and 24 μm below the surface of the sapphire substrate for all the samples. Furthermore, the amorphous sapphire in the sample fills the parabolic profile that is produced by the laser ablation. In all cases, the profile becomes more prominent after HF etching.

The morphology of the sample after HF etching depends on the exposure dose of the laser, since it was observed that more amorphous material remains at higher doses. Although the wet etching of sapphire is typically performed at higher temperatures, still some amount of amorphous material is removed at doses below 100 J/cm^2 at room temperature. The remaining amorphous material at the higher doses suggests that those particles may consist of a crystalline phase that formed during the laser ablation process.

The etching process provided excellent results for lines under 3.2 mW, where nearly 90% of the amorphous layer was removed. However, all lines above 40% contained a large portion of the amorphous layer. The depth and width of the patterned lines are plotted vs exposure dose in Figs. 4(a) and 4(b), respectively. While both the width and depth of the lines increase, the line width has a substantially smaller increase after HF etching compared to that of the depth. This shows that the write pattern in the laser setup impacts the depth of the features substantially more than that of the width, which is consistent with the width of the focal spot and the parabolic morphology of the features. On average, the width and depth of the sample increase by about 3 μm, and the amorphous layer is reduced by 30%. It is also observed that sometimes the amorphous region is not completely removed after the HF etching, which can be attributed to the material getting wedged into the parabolic trenches, as shown in Fig. 3(f).

B. PCA analysis of the OES signal

The goal of this work is to induce morphology changes in the sapphire without significant ablation damage, and therefore, the

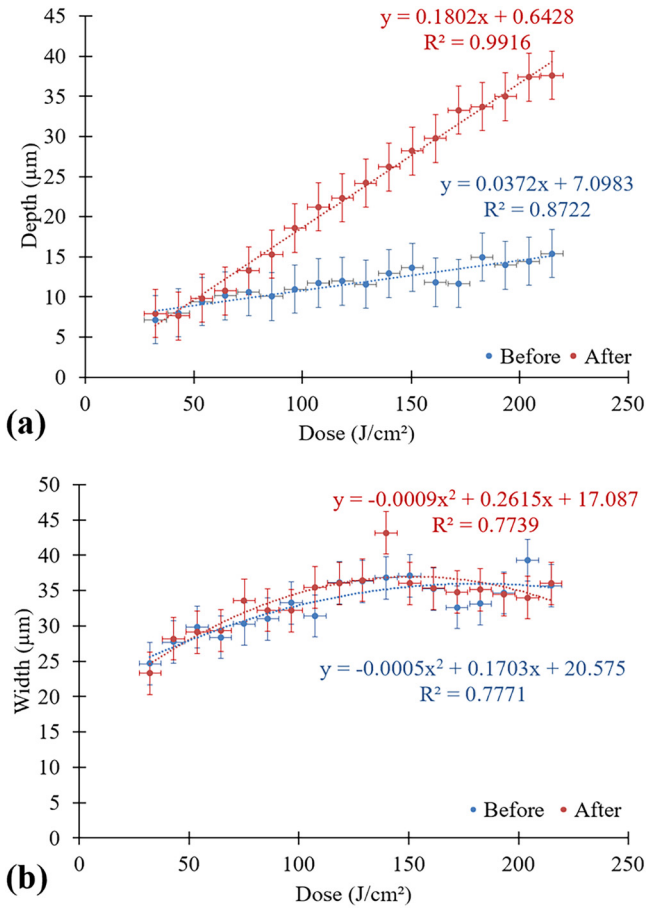

FIG. 4. (a) Depth and (b) width of the fabricated lines in sapphire before and after 10 min HF etching vs the patterning dose.

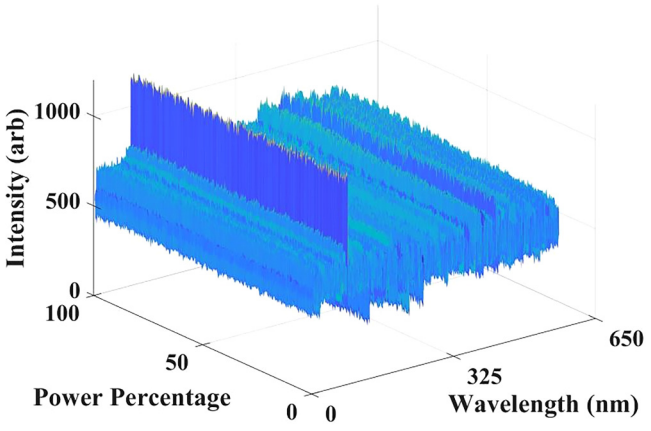

FIG. 5. Raw OES data of direct-write laser ablation on a sapphire substrate.

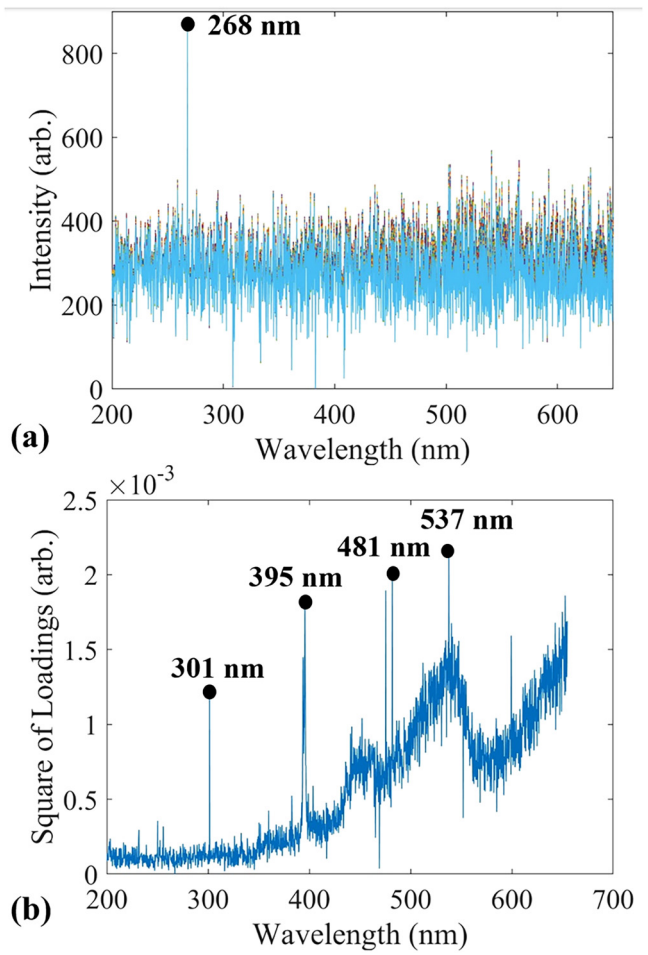

FIG. 6. Key wavelengths given by (a) the raw OES data and (b) the square of loadings from PCA result.

laser parameters used generates relatively weak emission spectra compared with laser-induced breakdown spectroscopy (LIBS) that is commonly used for material analysis.[26,27] As a result, the raw OES data collected require long integration time and contain a substantial amount of noise. Figure 5 shows the contour of the OES data collected, which plots the arbitrary intensity measured versus 200 to 650 nm wavelength and 0% to 100% nominal power of the laser. The noise of this data is reflected by the variation of the intensity, which makes it difficult to identify any trends in the data.

The raw OES data for each power and the result of the PCA analysis are plotted versus wavelength in Fig. 6. Here, a prominent peak in the raw OES data can be observed at approximately 268 nm, as shown in Fig. 6(a), which can be used as a key wavelength since it is notably higher in intensity than the surrounding wavelengths. However, once the PCA of the signal has been analyzed, several other wavelength peaks can be identified that are not noticeable in the raw data, as shown in Fig. 6(b). Here, the square

TABLE I. Key wavelengths identified via PCA vs NIST emission lines.

Key wavelength (nm)	Corresponding element and emission wavelength (nm) found in the NIST table
301	C II (299.3)
395	Al I (396.2)
481	N II (480.3)
537	C I (538.0)

of the loadings is plotted versus wavelength, and four notable peaks of 301, 395, 481, and 537 nm can be identified, as shown in Fig. 6(b). Based on basic atomic spectroscopic data provided by NIST,[28] 301 and 537 nm represent emissions of C, 481 nm represents emission of N, and 395 nm represents emission of Al. The detailed corresponding emission lines and elements found in the NIST table are shown in Table I. It is interesting to note there is no peak at 268 nm in the PCA data and no relevant emission lines can be identified from the NIST table, which suggests that the peak seen in the raw data is a result of noise. The slight difference between the NIST emission lines and key wavelengths identified via PCA can be attributed to the grating and calibration errors in the spectrometer. These peaks demonstrate the wavelengths that are most likely to have been emitted when the laser light interacted with the sapphire and surrounding gases, rather than noise from the instrumentation.

As a calibration study, we first want to examine the relationship between the set laser power and the measured OES signal at a particular wavelength, which can serve as a method to monitor the actual laser dosage at the substrate. Because sapphire is made of Al and O, which is included in the characteristic emission at 395 nm, this wavelength is used to compare with the strongest emission at 268 nm to confirm the validity of the PCA. Figure 7 compares the laser dose compared with the key wavelengths before and after PCA is conducted. Both signals are comparable and scale linearly

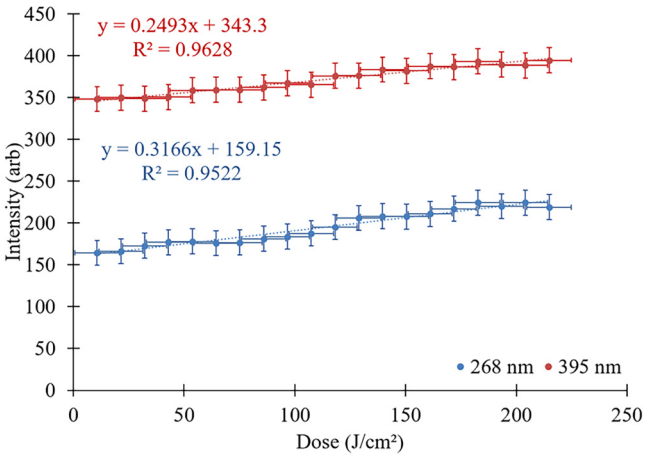

FIG. 7. OES results for dose vs intensity at 268 and 395 nm.

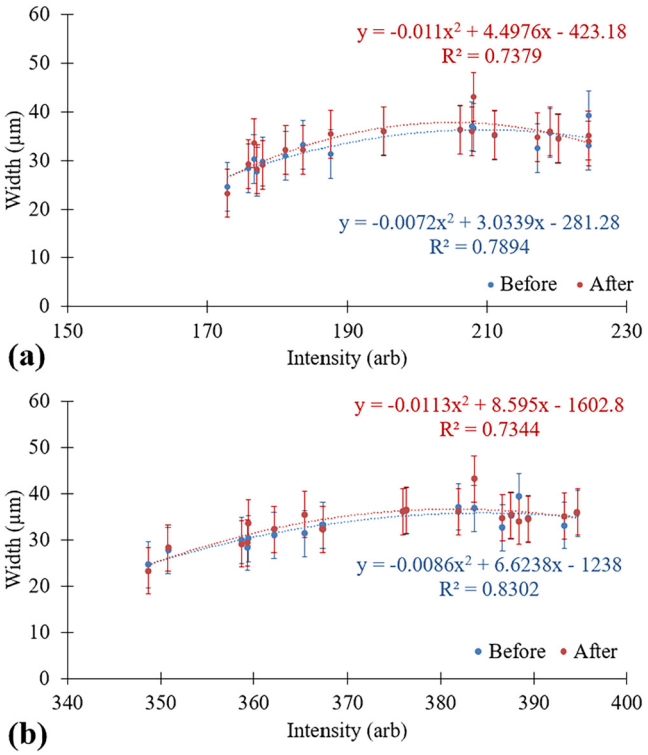

FIG. 8. Measured linewidth vs OES intensity before and after 10 min of HF etching at wavelengths of (a) 268 and (b) 395 nm.

with the laser dose, with an R^2 of 0.95 and 0.96 for the 268 and 395 nm wavelengths, respectively. However, without PCA, only 268 nm would be identified as a key wavelength, which would prevent a thorough assessment of the light–matter interactions by other wavelengths, including 395 nm. This result indicates that OES, in conjunction with data-driven PCA, can identify strong correlations between the emitted light and the direct-write laser ablation process.

Beyond monitoring the laser power at the substrate plane, the feature width before and after the HF etch can also be compared for both 268 and 395 nm to further determine the validity of OES and PCA. In Fig. 8, the line width and the intensity of the emitted light are compared for both wavelengths. For both before and after HF etching, both signals exhibit a strong quadratic correlation, where the width of fabricated trenches appears to reach a maximum and does not increase further with a higher dose. It can be observed that while the 268 nm wavelength signal shows high correlation to the regression model, with an R^2 of 0.79, it is less predictive of the features after HF etching with an R^2 of 0.74. On the other hand, the 395 nm wavelength intensity signal identified by PCA has a higher R^2 of 0.83 for the depth after HF etching, which is more relevant as the final parameter after both processes.

The line depth of the pattern trough and the intensity of the emitted light are also compared for 268 and 395 nm, which are

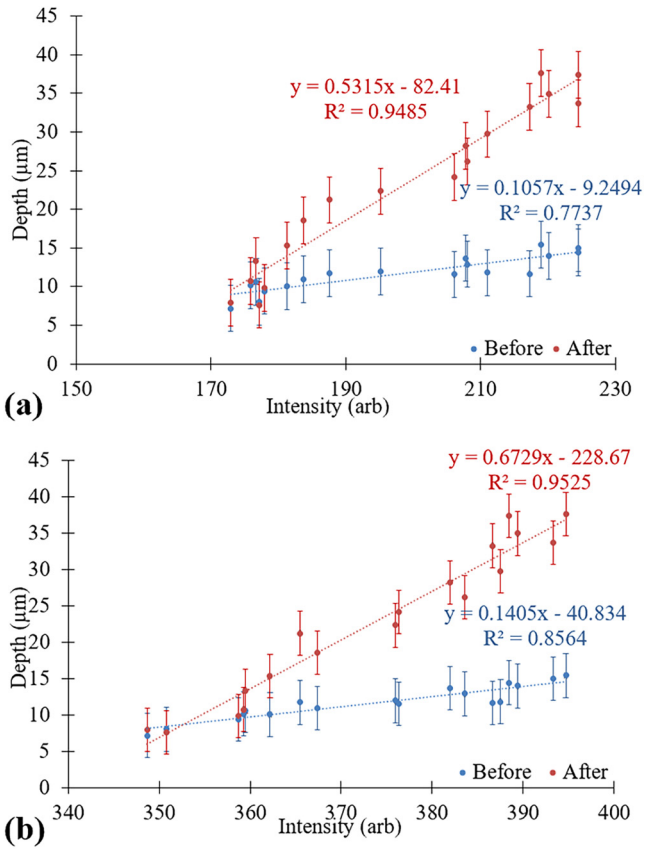

FIG. 9. Measured trough depth vs OES intensity before and after 10 min of HF etching at wavelengths of (a) 268 and (b) 395 nm.

shown in Fig. 9, which reveals increasing depth at higher intensity. It can be observed that the depth generally increases after the HF etching, which allows some of the residual amorphous alumina to be removed. Here, the linear regression R^2 results for 268 nm wavelength before and after HF etching are 0.77 and 0.95, respectively. The corresponding R^2 results for 395 nm identified by PCA before and after the HF etching are 0.86 and 0.95, respectively. It can be observed that the result from the depth correlation follows similar trends as in Fig. 8, with 395 nm demonstrating statistically more significant correlations between the line depth and the recorded intensity. Furthermore, the intensity at 295 nm compared with the feature morphology demonstrates similar correlations as that of 395 nm, which shows that the raw OES data can provide accurate correlations in real time during the laser ablation process. However, the wavelength identified using PCA has a slightly higher slope (0.67) compared with the characteristic emission (0.53) for the depth after HF etching, which indicates that monitoring the former would yield higher sensitivity.

These data provide some validation that the PCA of OES data can help identify key wavelength emissions that exhibit strong correlation to the fabricated microstructure in sapphire, although some challenges exist. The signal-to-noise ratio of the OES is a limiting factor, and the current experiments utilize a long integration time of one second for each measured spectrum. This limits the rate at which the metrology data can be measured and the process parameter to be updated. This bandwidth issue can be mitigated by using a high-sensitivity photodiode bandpass filtered at the identified key wavelengths, which can lead to a higher data acquisition rate. Future work also includes a further analysis of other key wavelengths identified by PCA, which even though are not aligned with relevant material emissions, may nevertheless provide some information on the fabricated structures. We also plan to implement this metrology system with real-time laser power control to enable real-time process control during the ablation process.

IV. CONCLUSION

This work demonstrates that the PCA of OES signals can identify key wavelengths that exhibit strong correlation to fabricated microstructures in direct-write ablation. The experiments demonstrate that the patterned line width, depth, and amorphous area grow significantly after HF etching, which increases the profile fidelity. The measured feature dimensions before and after HF etching and the associated OES data are analyzed with PCA, which identifies a key wavelength of 395 nm that exhibits strong correlations to patterned line width. The emission at 395 nm enables an accurate prediction of the pattern line width and depth with R^2 as high as 0.95 after HF etching. Based on the regression model developed, the emission from the key wavelength can be monitored *in situ* to reduce pattern inconsistency that pertains to specific morphologies by altering the laser power. This work can lead to real-time metrology and process control, which can improve the yield and repeatability of direct-write laser ablation for applications in nanophotonics, transparent ceramic windows, and flexible electronics.

ACKNOWLEDGMENTS

This work was performed at the UT Austin Texas Materials Institute (TMI), the Nanomanufacturing System for mobile Computing and Energy Technologies (NASCENT), and Texas Nanofabrication Facilities, which is supported by the National Science Foundation (NSF) as part of the National Nanotechnology Coordinated Infrastructure (NNCI) Grant No. NNCI-2025227. This work is funded by the Army Research Office (ARO) under Grant No. W911NF-22-1-0124.

AUTHOR DECLARATIONS

Conflict of Interest

The authors have no conflicts to disclose.

Author Contributions

Briana Cuero: Conceptualization (equal); Data curation (lead); Formal analysis (equal); Funding acquisition (equal); Investigation (equal); Methodology (equal); Project administration (equal); Resources (equal); Software (equal); Validation (equal); Visualization (lead); Writing – original draft (equal); Writing –

review & editing (equal). **Kun-Chieh Chien:** Conceptualization (equal); Data curation (supporting); Formal analysis (supporting); Funding acquisition (equal); Investigation (supporting); Methodology (supporting); Project administration (equal); Resources (supporting); Software (supporting); Supervision (supporting); Validation (supporting); Writing – original draft (supporting); Writing – review & editing (equal). **Chih-Hao Chang:** Conceptualization (lead); Formal analysis (supporting); Methodology (supporting); Project administration (lead); Resources (supporting); Supervision (lead); Validation (supporting); Visualization (supporting); Writing – review & editing (supporting).

DATA AVAILABILITY

The data that support the findings of this study are available from the corresponding author upon reasonable request.

REFERENCES

[1]H. W. Choi, D. F. Farson, J. Bovatsek, A. Arai, and D. Ashkenasi, Appl. Opt. **46**, 5792 (2007).
[2]M. Henry, P. M. Harrison, and J. Wendland, J. Laser Micro/Nanoeng. **2**, 49 (2007).
[3]A. Grushina, Adv. Opt. Technol. **8**, 163 (2019).
[4]G. Paris, D. Bierbaum, M. Paris, D. Mager, and F. F. Loeffler, Appl. Sci. **12**, 1361 (2022).
[5]R. S. Kappes, F. Schönfeld, C. Li, A. A. Golriz, M. Nagel, T. Lippert, H.-J. Butt, and J. S. Gutmann, SpringerPlus **3**, 489 (2014).
[6]B. Verhoff, S. S. Harilal, J. R. Freeman, P. K. Diwakar, and A. Hassanein, J. Appl. Phys. **112**, 093303 (2012).
[7]C. Geertsen, J.-L. Lacour, P. Mauchien, and L. Pierrard, Spectrochim. Acta, Part B **51**, 1403 (1996).
[8]A. De Giacomo, V. A. Shakhatov, and O. De Pascale, Spectrochim. Acta, Part B **56**, 753 (2001).
[9]C.-W. Chang, C.-Y. Chen, T.-L. Chang, C.-J. Ting, C.-P. Wang, and C.-P. Chou, Appl. Phys. A **109**, 441 (2012).
[10]S. Juodkazis, K. Nishimura, H. Misawa, T. Ebisui, R. Waki, S. Matsuo, and T. Okada, Adv. Mater. **18**, 1361 (2006).
[11]D. Wortmann, J. Gottmann, N. Brandt, and H. Horn-Solle, Opt. Express **16**, 1517 (2008).
[12]X. Q. Liu, S. N. Yang, L. Yu, Q. D. Chen, Y. L. Zhang, and H. B. Sun, Adv. Funct. Mater. **29**, 1900037 (2019).
[13]H. Park, K.-J. Byeon, J.-J. Jang, O. Nam, and H. Lee, Microelectron. Eng. **88**, 3207 (2011).
[14]H. Chen, Q. Zhang, and S. Y. Chou, Nanotechnology **26**, 085302 (2015).
[15]Y.-A. Chen, K.-C. Chien, I.-T. Chen, and C.-H. Chang, Micro Nano Eng. **14**, 100115 (2022).
[16]C. H. Jeong, D. W. Kim, H. Y. Lee, H. S. Kim, Y. J. Sung, and G. Y. Yeom, Surf. Coat. Technol. **171**, 280 (2003).
[17]Y. P. Hsu, S. J. Chang, Y. K. Su, J. K. Sheu, C. H. Kuo, C. S. Chang, and S. C. Shei, Opt. Mater. **27**, 1171 (2005).
[18]H. Liu, Y. Li, W. Lin, and M. Hong, Opt. Laser Technol. **132**, 106472 (2020).
[19]A. Polman, M. Kociak, and F. J. García de Abajo, Nat. Mater. **18**, 1158 (2019).
[20]C. Grimaldi, S. McGuire, A. C. Tibère-Inglesse, and C. O. Laux, *AIAA Scitech 2021 Forum* (American Institute of Aeronautics and Astronautics, 2021).
[21]F. Zacharatos, M. Makrygianni, R. Geremia, E. Biver, D. Karnakis, S. Leyder, D. Puerto, P. Delaporte, and I. Zergioti, Appl. Surf. Sci. **374**, 117 (2016).
[22]I. T. Jolliffe and J. Cadima, Philos. Trans. R. Soc. London, Ser. A **374**, 20150202 (2016).
[23]J. E. Jackson, *A User's Guide to Principal Components* (John Wiley & Sons, 2005).
[24]H. H. Yue, S. J. Qin, J. Wiseman, and A. Toprac, J. Vac. Sci. Technol. A **19**, 66 (2001).
[25]K.-C. Chien, C.-H. Chang, and D. Djurdjanovic, J. Vac. Sci. Technol. B **39**, 064003 (2021).
[26]F. J. Fortes, J. Moros, P. Lucena, L. M. Cabalín, and J. J. Laserna, Anal. Chem. **85**, 640 (2013).
[27]A. Elhassan, A. Giakoumaki, D. Anglos, G. M. Ingo, L. Robbiola, and M. A. Harith, Spectrochim. Acta, Part B **63**, 504 (2008).
[28]A. Kramida, Yu. Ralchenko, J. Reader, and NIST ASD Team (2022). NIST Atomic Spectra Database (version 5.10).